THE JOURNAL OF PHYSICAL CHEMISTRY A

pubs.acs.org/JPCA Article

How CuCl and $CuCl_2$ Insert into C−N Bonds of Diazo Compounds: An Electronic Structure and Mechanistic Study

Fengyu Li, John Zenghui Zhang, and Fei Xia*

Cite This: J. Phys. Chem. A 2020, 124, 2029−2035 Read Online

ACCESS | Metrics & More | Article Recommendations | Supporting Information

ABSTRACT: The transition-metal Cu catalysts CuCl and $CuCl_2$ have been widely employed to catalyze a series of chemical reactions with diazo compounds because of their high efficiency and selectivity. However, how to yield the active Cu carbene species from the Cu catalysts and diazo compounds still remains unclear. In this work, we performed a comprehensive theoretical investigation on the electronic structures of CuCl and $CuCl_2$ in solution. The results indicate that the most stable structures for CuCl and $CuCl_2$ are dimer and monomer, respectively. The C−N bond insertion of aryldiazoacetate by CuCl yields a stable bimetallic carbene species, which differs from the monometallic carbene generated from $CuCl_2$.

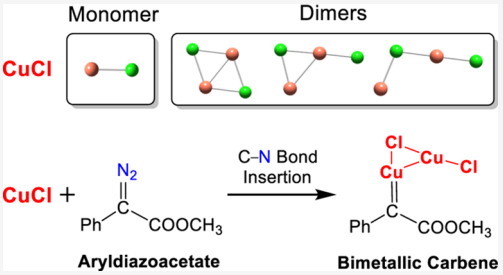

1. INTRODUCTION

Carbenes as reactive intermediates are extremely active so that they are widely used in chemical synthesis. Among them, the transition-metal carbenes are more prospective in the application to catalytic reactions due to their high catalytic efficiency and selectivity.[1−4] It is commonly accepted that they are generated by mixing metal catalysts with diazo compounds.[5] Metal carbenes such as Fe,[6] Au,[7−9] Rh,[10−19] and Cu[20−25] carbenes have been employed as active species to participate in a series of significant chemical reactions such as C−H bond functionalization,[26−31] O−H bond insertion,[32−34] cyclization,[35−38] and so on.[39−41] For example, Dai et al.[37] reported a cyclopropanation reaction of alkenes involved with Cu carbenes. Maier et al.[20] and Chen et al.[34] reported the enantioselective O−H functionalization of R−OH and phenols with Cu carbenes.

Apart from experimental reports, previous theoretical computations mainly focused on the mechanisms of reactions explicitly involving metal carbenes.[42−59] For example, Pei et al.[56] performed computational study on mechanisms of cyclization of indenes with Cu carbene. Liu et al.[54] calculated the pathways of the C−H and O−H bond insertions of phenols by Rh and Cu carbene. Fraile et al.[43] presented the mechanism study of a cyclopropanation reaction by Cu carbene with DFT calculations. Suess et al.[57] proposed the mechanisms of C−H functionalization of cyclic compounds catalyzed by Cu catalysts. Brandt et al.[58] elucidated the pathways of a Cu-catalyzed aziridination reaction of alkenes. Chen et al.[59] studied the mechanism of arylation of anilide at the meta position via a Cu intermediate. Although it is known that these metal carbenes are definitely involved in numerous significant reactions, the detailed mechanisms of how to generate the metal carbenes were seldom reported. Nakamura et al.[44] computed the insertion pathway of dirhodium tetracarboxylate into diazo compounds to generate Rh carbene. Liu et al.[52,53] calculated the pathways of gold ligands to insert into the C−N bond of diazo compounds to yield Au carbenes. As for the generation of Rh and Au carbenes aforementioned, it was well understood that they were generated from the direct C−N bond insertion of diazo compounds by the closed-shell Rh or Au metal catalysts.

Nevertheless, it maybe does not hold true for the generation of Cu carbenes that were generated from Cu catalysts with complicated electronic structures. Cuprous chloride (CuCl) and copper chloride ($CuCl_2$) are two of the most widely used Cu catalysts[3−5] in carbene generation. It is known that the electronic configurations of Cu and Cl atoms are $3d^{10}4s^1$ and $3s^23p^5$, respectively. The total number of electrons in the CuCl molecule is even, differing from the odd number of electrons in the single $CuCl_2$. This fact indicates that the CuCl is a closed-shell molecule, while $CuCl_2$ is an open-shell species. On the other hand, the Cu atoms in the monomers have more unsaturated sites, allowing multiple coordination with more chloride atoms. Thus, it could not be assumed that the generation of Cu carbene from CuCl and $CuCl_2$ follows a simple insertion mechanism.[44,52,53] The most stable structures of CuCl and $CuCl_2$ for the C−N bond insertion of diazo compounds in solution should be explored and clarified first before exploring the insertion mechanism.

Received: December 29, 2019
Revised: February 16, 2020
Published: February 21, 2020

https://dx.doi.org/10.1021/acs.jpca.9b11991
J. Phys. Chem. A 2020, 124, 2029−2035

In this work, we report a comprehensive density functional theory (DFT) calculation on the structures of the metal catalysts CuCl and $CuCl_2$ in solution as well as the reaction mechanism of insertion into the C−N bonds of diazo compounds. The possible mechanisms are shown in eqs 1−3:

$$2CuCl \rightleftarrows (CuCl)_2 \quad (1)$$

$$2CuCl_2 \leftrightarrows (CuCl_2)_2 \quad (2)$$

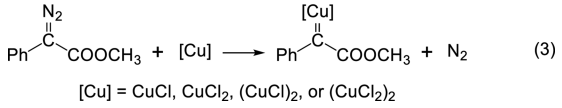

For simplicity, the aryldiazoacetate[14−16] molecule that is often used in reactions is chosen as the representative of diazo compounds in our DFT calculation. The mechanism of C−N bond insertion of aryldiazoacetate catalyzed by CuCl and $CuCl_2$ to generate the corresponding copper carbenes are uncovered based on DFT calculations.

2. COMPUTATIONAL METHODS

The DFT calculations throughout this work were carried out in the Gaussian09 program package.[60] All the structures of intermediates and transition states were optimized directly in the solution phase using the ωB97XD functional.[61] The large 6-31+G** basis set[62] is used for the nonmetallic H, C, O, N, and Cl elements, while the SDD basis set[63] combined with the pseudopotential is used to describe the metal element Cu. The combination of the ωB97XD functional and two basis sets is denoted as the ωB97XD/6-31+G**+SDD method. The unrestricted ωB97XD was employed to calculate the open-shell species. In addition, we also carried out single-point energy calculations on all optimized structures using the M06[64,65] functional for further comparison to the results of ωB97XD. The solvent effect of dichloromethane was evaluated using the IEFPCM model[66] in Gaussian09.

The frequency calculations were performed at the same level to validate whether the optimized structures were either local minima or transition states on the energy potential surface. All the energies presented in figures refer to the standard Gibbs free energies ΔG in solution, in the unit of kcal/mol at the temperature of 298.15 K. The intrinsic reaction coordinate (IRC)[67] calculations were performed to make sure that all the transition state structures connect the correct reactants and products. Nature bond orbital (NBO)[68] analysis was performed in Gaussian09 to elucidate the bonding interactions between the Cu and Cl atoms in the monomers and dimers of cuprous and copper chlorides.

3. RESULTS AND DISCUSSION

3.1. Structures of the Monomer and Dimers of CuCl.

In this section, we present the study on the stable structures of the monomer and dimers of CuCl by using DFT calculations. We analyze the bonding patterns and the electronic structures of optimized structures based on the NBO analysis and related occupied molecule orbitals (MOs), such as the highest occupied MO (HOMO). Figure 1a shows the optimized structures of monomer and dimers for CuCl and the corresponding free-energy profile for CuCl dimerization. The optimized monomer **MA1** is a simple linear closed-shell diatomic molecule with the bond length being 2.16 Å. The NBO analysis about the bonding in **MA1** reveals that the Cu−Cl bonding interaction is mainly contributed by 8.2% the *s*

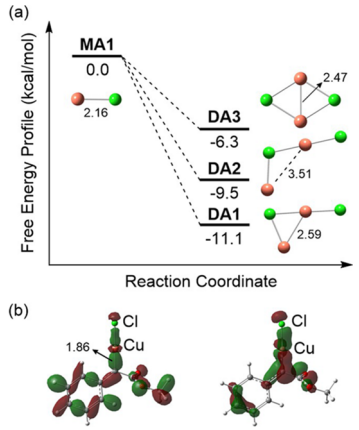

Figure 1. (a) Calculated energy profile for the dimerization of the CuCl monomer **MA1** to form the three dimers **DA1**, **DA2**, and **DA3**. (b) The plotted MOs of the metal carbene show the σ and π bonding interactions between the Cu and C atoms, respectively. The bond lengths are in angstrom.

orbital of Cu and 91.7% the *p* orbital of Cl, while the antibonding interaction comes from 91.7% the *s* orbital of Cu and 8.2% the *p* orbital of Cl. The CuCl monomer appears to be a metal coordination compound, rather than a typical covalent diatomic molecule. If **MA1** inserts into the C−N bond of diazo compounds to yield Cu carbene, the d_z^2 orbital of Cu overlaps with the sp^2 hybrid orbital of the carbon atom to form a σ-type bond, as shown in Figure 1b. Meanwhile, a conjugated π bond is also formed with the overlapping of the Cu *d* orbital and the carbon p_z orbital.

Owing to the unsaturated coordination of the Cu atom in CuCl, the monomer **MA1** is prone to form three different dimers, namely, the flag-shaped **DA1**, L-shaped **DA2**, and butterfly-shaped **DA3**, by releasing the energies of 11.1, 9.5, and 6.3 kcal/mol, respectively. By comparing the calculated relative free energies of the three dimers with each other, we find that the most stable dimer among them is the flag-shaped dimer **DA1** with the C_s symmetry. In **DA1**, the Cu−Cl−Cu angle is 71° and the Cu−Cu bond length is 2.59 Å. The second most stable dimer is the L-shaped **DA2** having a larger Cu−Cl−Cu angle of 106°. The energy of **DA2** is a little higher than that of **DA1** by 1.6 kcal/mol, while that of the butterfly-shaped **DA3** with the D_{2h} symmetry is even 4.8 kcal/mol higher than that of **DA1**. Actually, these three dimers might convert to each other in solution through bond breaking and electron rearrangement. For example, **DA1** could convert to the conformation of **DA2** by breaking the short Cu−Cu bond. Also, **DA1** could convert to **DA3** if it formed a new Cu−Cl bond. It is apparent that the electron configurations and bonding patterns in the three dimers differ distinctly from each other, which are originally caused by their specific geometrical structures.

It could be understood why the structure of **DA1** is more stable than **DA2** since the metal Cu−Cu bond plays an important role in stabilizing the structure of **DA1**. However, why is the structure **DA3** with the D_{2h} symmetry less stable than that of low-symmetry **DA1** in energy? To account for it, we plotted the two highest occupied MOs of **DA1** and **DA3** in Figure 2. It is obvious that the HOMO of **DA1** is a typical antibonding MO that destabilizes the whole structure. Nonetheless, the 35th MO of **DA1** shows that the two Cu atoms use two d orbitals to form an irregular weak δ bond to

https://dx.doi.org/10.1021/acs.jpca.9b11991
J. Phys. Chem. A 2020, 124, 2029−2035

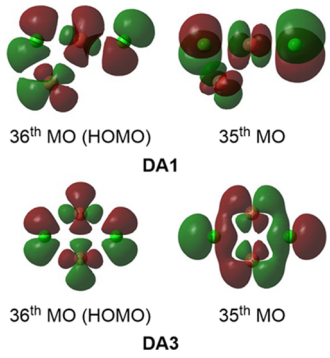

Figure 2. 36th HOMO and 35th MO of **DA1** and **DA3**, respectively.

strengthen the Cu−Cu interaction. In contrast, the 36th and 35th MOs of **DA3** are typical antibonding MOs in which the atomic orbitals of Cu and Cl could not form the effective bonding overlapping. The more occupied MOs of **DA1** and **DA3** are displayed in Figures S1 and S2 of the Supporting Information, respectively. The five highest occupied orbitals of **DA3** are characterized by the antibonding interactions, leading to the low stability of the **DA3** structure. Actually, the instability of MOs in **DA3** is indeed caused by its own high D_{2h} symmetry. In order to stabilize the whole system in energy, **DA3** must distort from the high D_{2h} symmetry to a structure with low symmetry C_s, such as that of **DA1**.

3.2. Structures of Monomers and Dimers of $CuCl_2$. As for $CuCl_2$, two monomers, **MB1** and **MB2**, were obtained from our DFT calculations, as shown in Figure 3a. The monomer

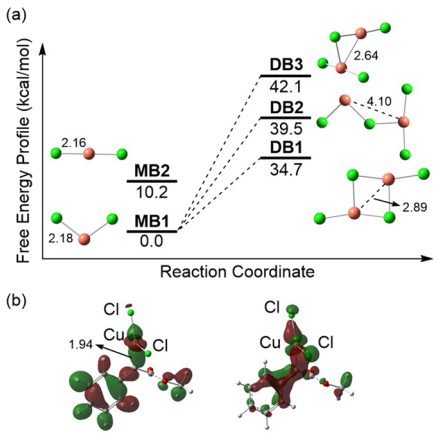

Figure 3. (a) Calculated two monomers **MB1** and **MB2** for $CuCl_2$ as well as the energy profile for the dimerization of **MB1** to form the three dimers **DB1**, **DB2**, and **DB3**. (b) The plotted MOs of the metal carbene show the σ and π bonding interactions between the Cu and C atoms. The bond lengths are in angstrom.

MB1 has a V-shaped structure with the C_{2v} symmetry, while the **MB2** is linear with the $D_{\infty h}$ symmetry. The energy of **MB1** is lower than that of **MB2** by 10.2 kcal/mol. The NBO analysis reveals that the hybrid type of Cl atoms in **MB1** is sp^3. Meanwhile, the central Cu atom adopts the dsp^2 hybridization, overlapping with the hybrid orbitals of Cl atoms. Figure 3b shows that **MB1** inserts into the C−N bond of the diazo compound and forms the metal carbene species. The left plot shows that one of the dsp^2 orbitals of Cu overlaps with one of the sp^2 orbitals of the C atom to form a σ bond, while the right plot shows a conjugated π bond formed by the d orbital of Cu and p_z orbital of the C atom. Thus, the Cu−C bond in the metal carbene is characterized by a double bond.

Another question that needs to be clarified is why the V-shaped **MB1** is more stable than the linear **MB2**. Figure 4

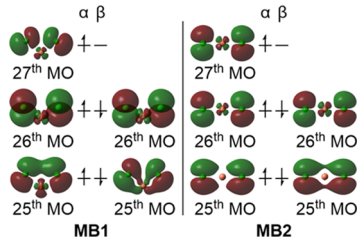

Figure 4. 27th, 26th, and 25th MOs occupied by α electrons and the 26th and 25th MOs occupied by β electrons for **MB1** and **MB2**, respectively.

shows the five highest MOs of **MB1** and **MB2** occupied by α and β electrons. It is obvious that the 26th and 27th MOs of both **MB1** and **MB2** are completely characterized by the antibonding orbital interactions. However, the p orbitals of Cl atoms in the α-electron 25th MO of **MB1** overlap with each other, so that the whole structure deviates from the linear. On the other hand, the 25th MO occupied by the β-electron exhibits a remarkable π bonding interaction between the d orbital of Cu and two p orbitals of Cl atoms, which strengthens the Cu−Cl bonding interaction to lower energy. In contrast, the 27th and 26th MOs of the linear **MB2** are antibonding MOs with strong repulsion interactions. Also, there is no effective overlapping between the d orbital of Cu and the two p orbitals of Cl atoms in the 25th MO of **MB2**. In a consequence, the overall bonding and antibonding interactions in **MB1** and **MB2** lead to the difference in stabilities. The more occupied MOs of **MB1** and **MB2** in Figure S3 of the Supporting Information also exhibit their difference in bonding and antibonding patterns.

Besides, we have calculated three dimers, **DB1**, **DB2**, and **DB3**, possibly formed from **MB1**. Our DFT calculations indicate that these dimers are quite unstable with the calculated energies being endothermic by 34.7, 39.5, and 42.1 kcal/mol, respectively. Therefore, it is almost impossible to form the three dimers in solution. Why are these structures of dimers quite unstable? In the case of **DB1**, the two highest occupied 53rd and 52nd MOs displayed in Figure 5 show that

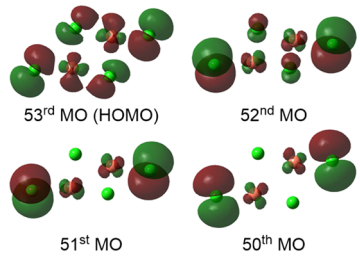

Figure 5. 53rd HOMO and 52nd, 51st, and 50th MOs of **DB1**.

the two MOs are characterized by the strong antibonding interactions between the atomic orbitals of Cu and Cl atoms. Therefore, the high C_{2h} symmetry of **DB1** renders it unstable in energy, similar to the situation of **DA3**.

3.3. Pathways of the Generation of Copper Carbene Using Catalytic CuCl. Before studying the insertion

https://dx.doi.org/10.1021/acs.jpca.9b11991
J. Phys. Chem. A 2020, 124, 2029−2035

mechanism, we first explore whether the aryldiazoacetate itself is ready to release N_2 directly at room temperature. The free-energy profile in Figure 6 shows that the direct dissociation of

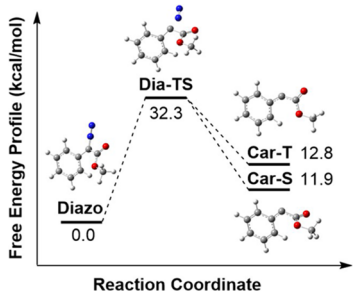

Figure 6. Calculated free energy profile for direct disassociation of N_2 from the diazo compound via the transition state **Dia-TS**, yielding the triplet **Car-T** and singlet **Car-S** species.

N_2 from the **Diazo** through the transition state **Dia-TS** has a high barrier of 32.3 kcal/mol. The release of N_2 possibly leads to two kinds of free carbenes, namely, **Car-S** in the singlet state and **Car-T** in the triplet state. Both their generations are endothermic by 11.9 and 12.8 kcal/mol, while the energy of **Car-T** is slightly higher than that of **Car-S** by 0.9 kcal/mol. The high kinetic barrier and endothermicity of the dissociation reaction indicate that it is difficult to occur spontaneously in solution. Thus, the direct dissociation of N_2 molecules from the aryldiazoacetate should be ignored, and the insertion mechanism of the C−N bond by the metal catalysts should be considered as a reasonable alternative. The DFT calculations in the last section demonstrate that CuCl exits in the form of dimers in solution. Thus, it is more reasonable to consider the dimers rather than the monomer to insert into the C−N bond of aryldiazoacetate.

Figure 7 shows the calculated energy profiles for the three dimers **DA1**, **DA2**, and **DA3** to insert into the C−N bonds of aryldiazoacetates. As what we discussed above, the precursors for the insertion reactions should involve the CuCl dimers as well as the aryldiazoacetate. In the first step, the **DA1** attaches to the central carbon atom of **Diazo** to form three stable intermediates, **DA1-1**, **DA2-1**, and **DA3-1**, by absorbing the energies of 7.0, 7.8, and 14.7 kcal/mol, respectively. The results of energy scanning indicate that no transition states exist for the Cu−C bond addition. Along the addition pathways, the central carbon atoms change their hybridization pattern from sp^2 to sp^3. The energy difference between **DA1-1** and **DA2-1** is merely 0.8 kcal/mol, which indicates that the transformation to each other is very feasible. It is noted that the flag-shaped **DA1-1** could convert to the L-shaped **DA2-1** by breaking the Cu−Cu bond in the dimer. As mentioned above, the Cu−Cu bonding in **DA1** is a weak δ-like bonding. The attachment of the terminal Cu to the carbene carbon in **DA1-1** weakens the δ bonding interaction between the terminal Cu and the middle Cu further, giving rise to the generation of **DA2-1**.

The subsequent dissociation of N_2 from **DA1-1**, **DA2-1**, and **DA3-1** needs to go through the transition states **DA1-TS**, **DA2-TS**, and **DA3-TS** with the calculated energies of 12.8, 14.4, and 24.5 kcal/mol, respectively. Comparing **DA1-TS** with the other two transition states, the energy is nearly endothermic by 12.8 kcal/mol, lower than that of **DA3-TS** by 11.7 kcal/mol. After releasing the N_2 molecule, the stable bimetallic carbene species[69] **DA1-2**, **DA2-2**, and **DA3-2** are yielded. The generation of the three metal carbenes is exothermic by 14.9, 14.2, and 5.6 kcal/mol, which indicates that they are quite stable in solution. If **DA1-2** yields the final monometallic carbene **DA-3** by dissociating a CuCl monomer, it needs the energy of 8.9 kcal/mol. We notice that the calculated length of the Cu−C bond in **DA1-2** is 1.87 Å, quite similar to the bond length of 1.86 Å in the monometallic

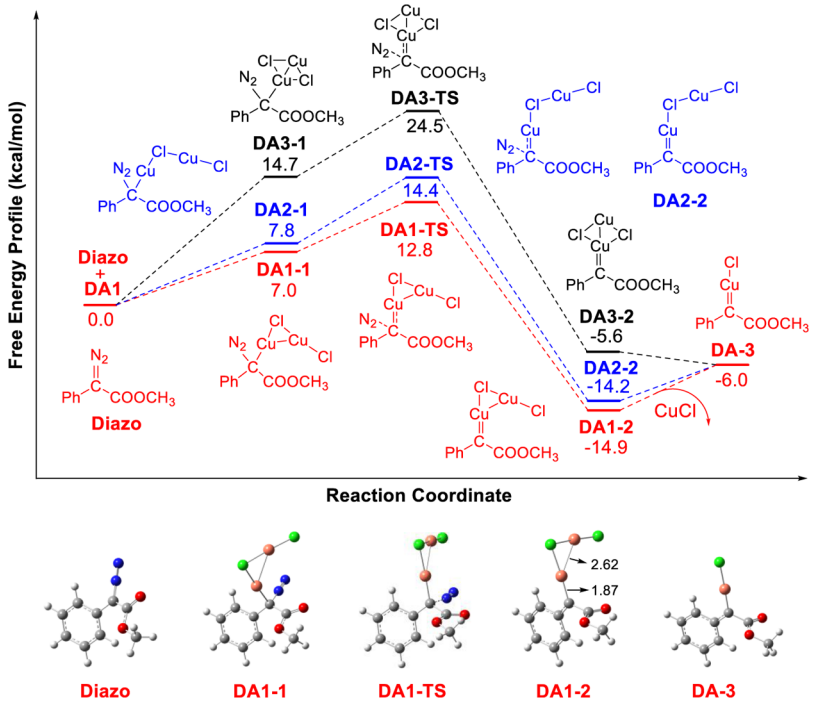

Figure 7. Calculated free energy profiles and structures for **DA1** to insert into the C−N bonds of aryldiazoacetates to yield the bimetallic carbenes. The bond lengths are in angstrom.

https://dx.doi.org/10.1021/acs.jpca.9b11991
J. Phys. Chem. A 2020, 124, 2029−2035

carbene **DA-3**. The MOs of **DA-3** in Figure 1b indicates the Cu−C bond of **DA-3** is a typical double bond. Thus, the Cu−C bond in **DA1−2** also indicates that it is a double metal−carbon bond. The comparison of the thermodynamic stability of **DA1-2** and **DA-3** indicates that the dominant metal carbene species resulted from the insertion reaction should be the bimetallic carbene **DA1-2**, rather than the general monometallic carbene species **DA-3**. **DA1-2** should be regarded as the active precursor to participate in the subsequent reactions. Besides, the insertion into the C−N bond of aryldiazoacetate by the monomer **MA1** is also calculated and presented in Figure S4 of the Supporting Information. Since the dimer **DA1** is more stable than the monomer **MA1**, the generation of **MA1** from **DA1** needs to absorb an energy of 11.1 kcal/mol. The whole kinetic barrier for the monomer insertion is high up to 21.7 kcal/mol, which is much less favorable than the insertion by **DA1** with the barrier of 12.8 kcal/mol.

3.4. Pathways of the Generation of Copper Carbene Using Catalytic $CuCl_2$. We also calculated the free-energy profile of the insertion of aryldiazoacetate by the $CuCl_2$ monomer **MB1**. Different from the case of CuCl, the monomer **MB1** is so stable that it is regarded as the reaction precursor. The calculated pathway is shown in Figure 8. The attachment

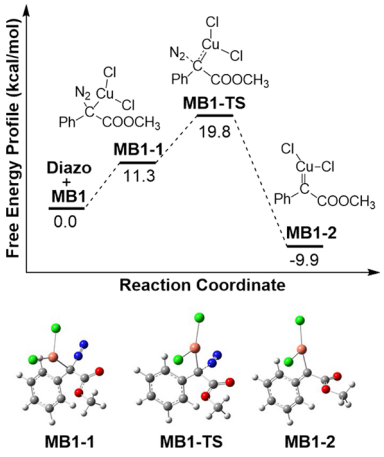

Figure 8. Calculated free energy profile for **MB1** to insert into the C−N bond of aryldiazoacetate to yield metal carbene **MB1-2**.

of **MB1** to the carbene carbon is endothermic by 11.3 kcal/mol to form the insertion intermediate **MB1-1**. Subsequently, the N_2 molecule is released from **MB1-1** via the transition state **MB1-TS**, giving the monometallic copper carbene **MB1-2** as the final product. The calculated Cu−C bond length in **MB1-2** is 1.94 Å, a little longer than that in **DA-3** by 0.08 Å. The barrier of the rate-determining step for this reaction is 19.8 kcal/mol, which means that the generation of **MB1-2** is feasible at room temperature.

It has to be mentioned that Cu(II) species such as $CuCl_2$ might be reduced to CuCl by the diazo compounds, as what has been observed in the previous reactions between aryldiazoacetates and copper species.[70,71] In the $CuCl_2$-catalyzed reaction, if the $CuCl_2$ catalyst was partially reduced to CuCl, the insertion into the C−N bond of aryldiazoacetate would follow the mechanism shown in Figure 7, which led to the bimetallic carbene **DA1-2** finally. On the other hand, in the CuCl-catalyzed reaction, if CuCl was partially oxidized to $CuCl_2$, the reaction still followed the mechanism in Figure 7. The reason lies in the fact that the calculated kinetic barrier for the CuCl insertion is lower than that of $CuCl_2$ by 7.0 kcal/mol. The reaction pathways of CuCl are more favorable in energy than those of $CuCl_2$, so the Cu(I) carbenes might be dominant in the final insertion products.

4. CONCLUSIONS

We performed a comprehensive DFT study and electronic structure analysis on the stable structures of CuCl and $CuCl_2$ in solution. It is found that CuCl prefers the dimer to the monomer in solution. Three possible stable dimers including the butterfly-shaped, L-shaped, and flag-shaped structures were obtained from DFT calculations. The flag-shaped dimer is the most stable one in energy among them. Through the MO bonding patterns and NBO analyses, we explain the reason why the structure of the flag-shaped dimer is the most stable one.

Further, the reaction mechanisms of C−N bond insertion of aryldiazoacetates catalyzed by CuCl and $CuCl_2$ are investigated. The reaction pathways for the CuCl dimer and $CuCl_2$ monomer to insert into the C−N bonds of aryldiazoacetates were calculated and presented in figures with the details. The DFT results indicate that the inserted product catalyzed by CuCl might be the bimetallic carbene **DA1-2**, rather than the monometallic carbene species **DA-3**. For the insertion reaction catalyzed by $CuCl_2$, the V-shaped monomer **MB1** was inserted into the C−N bond of aryldiazoacetate to yield the metal carbene **MB1-2**. The calculated results using the M06 method shown in Figures S5−S10 of the Supporting Information also support the conclusions. The calculated active carbene species **DA1-2** and **MB1** in this study should be regarded as the precursors in the carbene-participated reactions catalyzed by CuCl and $CuCl_2$.

■ ASSOCIATED CONTENT

Supporting Information

The Supporting Information is available free of charge at https://pubs.acs.org/doi/10.1021/acs.jpca.9b11991.

More occupied MOs (Figures S1−S3), free-energy profile for MA1 insertion (Figure S4), results of M06 (Figures S5−S10), and computed absolute energies and Cartesian coordinates of all the optimized structures in figures (PDF)

■ AUTHOR INFORMATION

Corresponding Author

Fei Xia − *Shanghai Engineering Research Center of Molecular Therapeutics and New Drug Development, School of Chemistry and Molecular Engineering and NYU-ECNU Center for Computational Chemistry at New York University Shanghai, East China Normal University, Shanghai 200062, China;* orcid.org/0000-0001-9458-9175; Phone: +86-(0)21-20596009; Email: fxia@chem.ecnu.edu.cn

Authors

Fengyu Li − *Shanghai Engineering Research Center of Molecular Therapeutics and New Drug Development, School of Chemistry and Molecular Engineering, East China Normal University, Shanghai 200062, China*

John Zenghui Zhang − *Shanghai Engineering Research Center of Molecular Therapeutics and New Drug Development, School of Chemistry and Molecular Engineering and NYU-ECNU Center for Computational Chemistry at New York University*

Shanghai, East China Normal University, Shanghai 200062, China; orcid.org/0000-0003-4612-1863

Complete contact information is available at: https://pubs.acs.org/10.1021/acs.jpca.9b11991

Notes

The authors declare no competing financial interest.

■ ACKNOWLEDGMENTS

This work was supported by the National Natural Science Foundation of China (grant nos. 21433004 and 21773065). We acknowledge the support of the NYU-ECNU Center for Computational Chemistry at NYU Shanghai. We also thank the ECNU Multifunctional Platform for Innovation(001) for providing computer time.

■ REFERENCES

(1) Cardin, D. J.; Cetinkaya, B.; Lappert, M. F. Transition Metal-Carbene Complexes. *Chem. Rev.* **1972**, *72*, 545−574.
(2) Dötz, K. H. Carbene Complexes in Organic Synthesis [New Synthetic Methods (47)]. *Angew. Chem., Int. Ed. Engl.* **1984**, *23*, 587−608.
(3) Doyle, M. P.; Forbes, D. C. Recent Advances in Asymmetric Catalytic Metal Carbene Transformations. *Chem. Rev.* **1998**, *98*, 911−936.
(4) Doyle, M. P.; Duffy, R.; Ratnikov, M.; Zhou, L. Catalytic Carbene Insertion into C−H Bonds. *Chem. Rev.* **2010**, *110*, 704−724.
(5) Doyle, M. P. Catalytic Methods for Metal Carbene Transformations. *Chem. Rev.* **1986**, *86*, 919−939.
(6) Mbuvi, H. M.; Woo, L. K. Catalytic C−H Insertions Using Iron(III) Porphyrin Complexes. *Organometallics* **2008**, *27*, 637−645.
(7) Rivilla, I.; Gómez-Emeterio, B. P.; Fructos, M. R.; Díaz-Requejo, M. M.; Pérez, P. J. Exclusive Aromatic *vs* Aliphatic C−H Bond Functionalization by Carbene Insertion with Gold-Based Catalysts. *Organometallics* **2011**, *30*, 2855−2860.
(8) Yu, Z.; Ma, B.; Chen, M.; Wu, H. H.; Liu, L.; Zhang, J. Highly Site-Selective Direct C−H Bond Functionalization of Phenols with α-Aryl-α-diazoacetates and Diazooxindoles via Gold Catalysis. *J. Am. Chem. Soc.* **2014**, *136*, 6904−6907.
(9) Xi, Y.; Su, Y.; Yu, Z.; Dong, B.; McClain, E. J.; Lan, Y.; Shi, X. Chemoselective Carbophilic Addition of α-Diazoesters through Ligand-Controlled Gold Catalysis. *Angew. Chem., Int. Ed.* **2014**, *53*, 9817−9821.
(10) Padwa, A.; Austin, D. J.; Price, A. T.; Semones, M. A.; Doyle, M. P.; Protopopova, M. N.; Winchester, W. R.; Tran, A. Ligand Effects on Dirhodium(II) Carbene Reactivities. Highly Effective Switching between Competitive Carbenoid Transformations. *J. Am. Chem. Soc.* **1993**, *115*, 8669−8680.
(11) Wood, J. L.; Moniz, G. A.; Pflum, D. A.; Stoltz, B. M.; Holubec, A. A.; Dietrich, H.-J. Development of a Rhodium Carbenoid-Initiated Claisen Rearrangement for the Enantioselective Synthesis of α-Hydroxy Carbonyl Compounds. *J. Am. Chem. Soc.* **1999**, *121*, 1748−1749.
(12) Wood, J. L.; Moniz, G. A. Rhodium Carbenoid-Initiated Claisen Rearrangement: Scope and Mechanistic Observations. *Org. Lett.* **1999**, *1*, 371−374.
(13) Doyle, M. P.; Yan, M. Chiral Catalyst Enhancement of Diastereocontrol for O−H Insertion Reactions of Styryl- and Phenyldiazoacetate Esters of Pantolactone. *Tetrahedron Lett.* **2002**, *43*, 5929−5931.
(14) Wang, Y.; Zhu, Y.; Chen, Z.; Mi, A.; Hu, W.; Doyle, M. P. A Novel Three-Component Reaction Catalyzed by Dirhodium(II) Acetate: Decomposition of Phenyldiazoacetate with Arylamine and Imine for Highly Diastereoselective Synthesis of 1,2-Diamines. *Org. Lett.* **2003**, *5*, 3923−3926.
(15) Liao, M.; Wang, J. Highly Efficient [2,3]-Sigmatropic Rearrangement of Sulfur Ylide Derived from Rh(II) Carbene and Sulfides in Water. *Green Chem.* **2007**, *9*, 184−188.
(16) Huang, H.; Guo, X.; Hu, W. Efficient Trapping of Oxonium Ylides with Imines: A Highly Diastereoselective Three-Component Reaction for the Synthesis of β-Amino-α-hydroxyesters with Quaternary Stereocenters. *Angew. Chem., Int. Ed.* **2007**, *46*, 1337−1339.
(17) Hu, W.; Xu, X.; Zhou, J.; Liu, W.-J.; Huang, H.; Hu, J.; Yang, L.; Gong, L.-Z. Cooperative Catalysis with Chiral Brønsted Acid-$Rh_2(OAc)_4$: Highly Enantioselective Three-Component Reactions of Diazo Compounds with Alcohols and Imines. *J. Am. Chem. Soc.* **2008**, *130*, 7782−7783.
(18) Li, Z.; Davies, H. M. L. Enantioselective C−C Bond Formation by Rhodium-Catalyzed Tandem Ylide Formation/[2,3]-Sigmatropic Rearrangement between Donor/Acceptor Carbenoids and Allylic Alcohols. *J. Am. Chem. Soc.* **2010**, *132*, 396−401.
(19) Li, Z.; Parr, B. T.; Davies, H. M. L. Highly Stereoselective C−C Bond Formation by Rhodium-Catalyzed Tandem Ylide Formation/[2,3]-Sigmatropic Rearrangement between Donor/Acceptor Carbenoids and Chiral Allylic Alcohols. *J. Am. Chem. Soc.* **2012**, *134*, 10942−10946.
(20) Maier, T. C.; Fu, G. C. Catalytic Enantioselective O−H Insertion Reactions. *J. Am. Chem. Soc.* **2006**, *128*, 4594−4595.
(21) Lebel, H.; Davi, M.; Díez-González, S.; Nolan, S. P. Copper-Carbene Complexes as Catalysts in the Synthesis of Functionalized Styrenes and Aliphatic Alkenes. *J. Org. Chem.* **2007**, *72*, 144−149.
(22) Cao, H.; Jiang, H.; Yao, W.; Liu, X. Copper-Catalyzed Domino Rearrangement/Dehydrogenation Oxidation/Carbene Oxidation for One-Pot Regiospecific Synthesis of Highly Functionalized Polysubstituted Furans. *Org. Lett.* **2009**, *11*, 1931−1933.
(23) Citadelle, C. A.; Nouy, E. L.; Bisaro, F.; Slawin, A. M. Z.; Cazin, C. S. J. Simple and Versatile Synthesis of Copper and Silver N-Heterocyclic Carbene Complexes in Water or Organic Solvents. *Dalton Trans.* **2010**, *39*, 4489−4491.
(24) Hu, M.; He, Z.; Gao, B.; Li, L.; Ni, C.; Hu, J. Copper-Catalyzed *gem*-Difluoroolefination of Diazo Compounds with $TMSCF_3$ via C−F Bond Cleavage. *J. Am. Chem. Soc.* **2013**, *135*, 17302−17305.
(25) Zhang, H.; Wu, G.; Yi, H.; Sun, T.; Wang, B.; Zhang, Y.; Dong, G.; Wang, J. Copper(I)-Catalyzed Chemoselective Coupling of Cyclopropanols with Diazoesters: Ring-Opening C−C Bond Formations. *Angew. Chem., Int. Ed.* **2017**, *56*, 3945−3950.
(26) Davies, H. M. L.; Manning, J. R. Catalytic C−H Functionalization by Metal Carbenoid and Nitrenoid Insertion. *Nature* **2008**, *451*, 417−424.
(27) Davies, H. M. L.; Morton, D. Guiding Principles for Site Selective and Stereoselective Intermolecular C−H Functionalization by Donor/Acceptor Rhodium Carbenes. *Chem. Soc. Rev.* **2011**, *40*, 1857−1869.
(28) DeAngelis, A.; Shurtleff, V. W.; Dmitrenko, O.; Fox, J. M. Rhodium(II)-Catalyzed Enantioselective C−H Functionalization of Indoles. *J. Am. Chem. Soc.* **2011**, *133*, 1650−1653.
(29) Zhu, S.-F.; Zhou, Q.-L. Transition-Metal-Catalyzed Enantioselective Heteroatom−Hydrogen Bond Insertion Reactions. *Acc. Chem. Res.* **2012**, *45*, 1365−1377.
(30) Jiménez-Osés, G.; Vispe, E.; Roldán, M.; Rodríguez-Rodríguez, S.; López-Ram-de-Viu, P.; Salvatella, L.; Mayoral, J. A.; Fraile, J. M. Stereochemical Outcome of Copper-Catalyzed C−H Insertion Reactions. An Experimental and Theoretical Study. *J. Org. Chem.* **2013**, *78*, 5851−5857.
(31) Liao, K.; Yang, Y. F.; Li, Y.; Sanders, J. N.; Houk, K. N.; Musaev, D. G.; Davies, H. M. L. Design of Catalysts for Site-Selective and Enantioselective Functionalization of Non-Activated Primary C−H Bonds. *Nature Chem.* **2018**, *10*, 1048−1055.
(32) Miller, D. J.; Moody, C. J. Synthetic Applications of the O−H Insertion Reactions of Carbenes and Carbenoids Derived from Diazocarbonyl and Related Diazo Compounds. *Tetrahedron* **1995**, *51*, 10811−10843.

(33) Lu, C. D.; Liu, H.; Chen, Z.-Y.; Hu, W.-H.; Mi, A.-Q. Three-Component Reaction of Aryl Diazoacetates, Alcohols, and Aldehydes (or Imines): Evidence of Alcoholic Oxonium Ylide Intermediates. *Org. Lett.* **2005**, *7*, 83−86.
(34) Chen, C.; Zhu, S. F.; Liu, B.; Wang, L. X.; Zhou, Q. L. Highly Enantioselective Insertion of Carbenoids into O−H Bonds of Phenols: An Efficient Approach to Chiral α-Aryloxycarboxylic Esters. *J. Am. Chem. Soc.* **2007**, *129*, 12616−12617.
(35) Doyle, M. P.; Tamblyn, W. H.; Bagheri, V. Highly Effective Catalytic Methods for Ylide Generation from Diazo Compounds. Mechanism of the Rhodium- and Copper-Catalyzed Reactions with Allylic Compounds. *J. Org. Chem.* **1981**, *46*, 5094−5102.
(36) Lebel, H.; Marcoux, J. F.; Molinaro, C.; Charette, A. B. Stereoselective Cyclopropanation Reactions. *Chem. Rev.* **2003**, *103*, 977−1050.
(37) Dai, X.; Warren, T. H. Discrete Bridging and Terminal Copper Carbenes in Copper-Catalyzed Cyclopropanation. *J. Am. Chem. Soc.* **2004**, *126*, 10085−10094.
(38) Ebner, C.; Carreira, E. M. Cyclopropanation Strategies in Recent Total Syntheses. *Chem. Rev.* **2017**, *117*, 11651−11679.
(39) Vedejs, E.; Hagen, J. P. Macrocycle Synthesis by Repeatable 2,3-Sigmatropic Shifts. Ring-Growing Reactions. *J. Am. Chem. Soc.* **1975**, *97*, 6878−6880.
(40) Urbano, J.; Braga, A. A. C.; Maseras, F.; Álvarez, E.; Díaz-Requejo, M. M.; Pérez, P. J. The Mechanism of the Catalytic Functionalization of Haloalkanes by Carbene Insertion: An Experimental and Theoretical Study. *Organometallics* **2009**, *28*, 5968−5981.
(41) Xia, Y.; Qiu, D.; Wang, J. Transition-Metal-Catalyzed Cross-Couplings through Carbene Migratory Insertion. *Chem. Rev.* **2017**, *117*, 13810−13889.
(42) Padwa, A.; Snyder, J. P.; Curtis, E. A.; Sheehan, S. M.; Worsencroft, K. J.; Kappe, C. O. Rhodium(II)-Catalyzed Equilibration of Push-Pull Carbonyl and Ammonium Ylides. A Computationally Based Understanding of the Reaction Pathway. *J. Am. Chem. Soc.* **2000**, *122*, 8155−8167.
(43) Fraile, J. M.; García, J. I.; Martínez-Merino, V.; Mayoral, J. A.; Salvatella, L. Theoretical (DFT) Insights into the Mechanism of Copper-Catalyzed Cyclopropanation Reactions. Implications for Enantioselective Catalysis. *J. Am. Chem. Soc.* **2001**, *123*, 7616−7625.
(44) Nakamura, E.; Yoshikai, N.; Yamanaka, M. Mechanism of C−H Bond Activation/C−C Bond Formation Reaction between Diazo Compound and Alkane Catalyzed by Dirhodium Tetracarboxylate. *J. Am. Chem. Soc.* **2002**, *124*, 7181−7192.
(45) Nowlan, D. T.; Gregg, T. M.; Davies, H. M. L.; Singleton, D. A. Isotope Effects and the Nature of Selectivity in Rhodium-Catalyzed Cyclopropanations. *J. Am. Chem. Soc.* **2003**, *125*, 15902−15911.
(46) Braga, A. A. C.; Maseras, F.; Urbano, J.; Caballero, A.; Díaz-Requejo, M. M.; Pérez, P. J. Mechanism of Alkane C−H Bond Activation by Copper and Silver Homoscorpionate Complexes. *Organometallics* **2006**, *25*, 5292−5300.
(47) Hansen, J.; Autschbach, J.; Davies, H. M. L. Computational Study on the Selectivity of Donor/Acceptor-Substituted Rhodium Carbenoids. *J. Org. Chem.* **2009**, *74*, 6555−6563.
(48) Liang, Y.; Zhou, H.; Yu, Z.-X. Why Is Copper(I) Complex More Competent Than Dirhodium(II) Complex in Catalytic Asymmetric O−H Insertion Reactions? A Computational Study of the Metal Carbenoid O−H Insertion into Water. *J. Am. Chem. Soc.* **2009**, *131*, 17783−17785.
(49) Bonge, H. T.; Hansen, T. Computational Study of C−H Insertion Reactions with Ethyl Bromodiazoacetate. *Eur. J. Org. Chem.* **2010**, 4355−4359.
(50) Bonge, H. T.; Hansen, T. Computational Study of Cyclopropanation Reactions with Halodiazoacetates. *J. Org. Chem.* **2010**, *75*, 2309−2320.
(51) Xie, Z.-Z.; Liao, W.-J.; Cao, J.; Guo, L.-P.; Verpoort, F.; Fang, W. Mechanistic Insight into the Rhodium-Catalyzed O−H Insertion Reaction: A DFT Study. *Organometallics* **2014**, *33*, 2448−2456.
(52) Liu, Y.; Yu, Z.; Luo, Z.; Zhang, J. Z.; Liu, L.; Xia, F. Mechanistic Investigation of Aromatic C(sp^2)−H and Alkyl C(sp^3)−H Bond Insertion by Gold Carbenes. *J. Phys. Chem. A* **2016**, *120*, 1925−1932.
(53) Liu, Y.; Yu, Z.; Zhang, J. Z.; Liu, L.; Xia, F.; Zhang, J. Origins of Unique Gold-Catalysed Chemo- and Site-Selective C−H Functionalization of Phenols with Diazo Compounds. *Chem. Sci.* **2016**, *7*, 1988−1995.
(54) Liu, Y.; Luo, Z.; Zhang, J. Z.; Xia, F. DFT Calculations on the Mechanism of Transition-Metal-Catalyzed Reaction of Diazo Compounds with Phenols: O−H Insertion versus C−H Insertion. *J. Phys. Chem. A* **2016**, *120*, 6485−6492.
(55) Luo, Z.; Gao, Y.; Zhu, T.; Zhang, J. Z.; Xia, F. Origins of Protons in C−H Bond Insertion Products of Phenols: Proton-Self-Sufficient Function via Water Molecules. *J. Phys. Chem. A* **2017**, *121*, 6523−6529.
(56) Pei, C.; Rong, G. W.; Yu, Z. X.; Xu, X. F. Copper-Catalyzed Intramolecular Annulation of Conjugated Enynones to Substituted 1*H*-Indenes and Mechanistic Studies. *J. Org. Chem.* **2018**, *83*, 13243−13255.
(57) Suess, A. M.; Ertem, M. Z.; Cramer, C. J.; Stahl, S. S. Divergence between Organometallic and Single-Electron-Transfer Mechanisms in Copper(II)-Mediated Aerobic C−H Oxidation. *J. Am. Chem. Soc.* **2013**, *135*, 9797−9804.
(58) Brandt, P.; Södergren, M. J.; Andersson, P. G.; Norrby, P.-O. Mechanistic Studies of Copper-Catalyzed Alkene Aziridination. *J. Am. Chem. Soc.* **2000**, *122*, 8013−8020.
(59) Chen, B.; Hou, X.-L.; Li, Y.-X.; Wu, Y.-D. Mechanistic Understanding of the Unexpected Meta Selectivity in Copper-Catalyzed Anilide C−H Bond Arylation. *J. Am. Chem. Soc.* **2011**, *133*, 7668−7671.
(60) Frisch, M. J.; Trucks, G. W.; Schlegel, H. B.; Scuseria, G. E.; Robb, M. A.; Cheeseman, J. R.; Scalmani, G.; Barone, V.; Mennucci, B.; Petersson, G. A.; et al. *Gaussian 09*; Gaussian, Inc.: Wallingford, CT, 2009.
(61) Chai, J.-D.; Head-Gordon, M. Long-Range Corrected Hybrid Density Functionals with Damped Atom-Atom Dispersion Corrections. *Phys. Chem. Chem. Phys.* **2008**, *10*, 6615−6620.
(62) Hehre, W. J.; Ditchfield, R.; Pople, J. A. Self-Consistent Molecular Orbital Methods. XII. Further Extensions of Gaussian-Type Basis Sets for Use in Molecular Orbital Studies of Organic Molecules. *J. Chem. Phys.* **1972**, *56*, 2257−2261.
(63) Dolg, M.; Wedig, U.; Stoll, H.; Preuss, H. Energy-Adjusted ab Initio Pseudopotentials for the First Row Transition Elements. *J. Chem. Phys.* **1987**, *86*, 866−872.
(64) Zhao, Y.; Truhlar, D. G. The M06 Suite of Density Functionals for Main Group Thermochemistry, Thermochemical Kinetics, Noncovalent Interactions, Excited States, and Transition Elements: Two New Functionals and Systematic Testing of Four M06-Class Functionals and 12 Other Functionals. *Theor. Chem. Acc.* **2008**, *120*, 215−241.
(65) Zhao, Y.; Truhlar, D. G. Density Functionals with Broad Applicability in Chemistry. *Acc. Chem. Res.* **2008**, *41*, 157−167.
(66) Scalmani, G.; Frisch, M. J. Continuous Surface Charge Polarizable Continuum Models of Solvation. I. General Formalism. *J. Chem. Phys.* **2010**, *132*, 114110.
(67) Fukui, K. The Path of Chemical Reactions - The IRC Approach. *Acc. Chem. Res.* **1981**, *14*, 363−368.
(68) Glendening, E. D.; Reed, A. E.; Carpenter, J. E.; Weinhold, F., *NBO version 3.1*; ScienceOpen, Inc., 2001.
(69) Xia, F.; Chen, J.; Zeng, K.; Cao, Z. Density Functional Characterization of Reactions of Bimetallic Carbenes $PtMCH_2^+$ (M = Pt, Au) with NH_3 in the Gas Phase. *Organometallics* **2005**, *24*, 1845−1851.
(70) Salomon, R. G.; Kochi, J. K. Cationic Olefin Complexes of Copper(I) . Structure and Bonding in Group Ib Metal-Olefin Complexes. *J. Am. Chem. Soc.* **1973**, *95*, 1889−1897.
(71) Salomon, R. G.; Kochi, J. K. Copper(I) catalysis in cyclopropanations with diazo compounds. Role of olefin coordination. *J. Am. Chem. Soc.* **1973**, *95*, 3300−3310.

https://dx.doi.org/10.1021/acs.jpca.9b11991
J. Phys. Chem. A 2020, 124, 2029−2035